6-22-2009

Oxidative Dehydrogenation of an Amine Group of a Macrocyclic Ligand in the Coordination Sphere of a Cu^{II} Complex

Gemma J. Christian
Avondale College, gemma.christian@avondale.edu.au

Arnau Arbuse
Universitat de Girona

Xavier Fontrodona
Universitat de Girona

Ma Angeles Martinez
Universitat de Girona

Antoni Llobet
Institute of Chemical Research of Catalonia

See next page for additional authors

Recommended Citation

Christian, G. J., Arbuse, A., Fontrodona, X., Martinez, M. A., Llobet, A., & Maseras, F. (2009). Oxidative dehydrogenation of an amine group of a macrocyclic ligand in the coordination sphere of a CuII complex. *Dalton Transactions, 2009*(30), 6013–6020. doi:10.1039/B902947H

Oxidative dehydrogenation of an amine group of a macrocyclic ligand in the coordination sphere of a Cu^{II} complex†

Gemma J. Christian,[a] Arnau Arbuse,[b] Xavier Fontrodona,[b] Ma Angeles Martinez,*[b] Antoni Llobet*[a,c] and Feliu Maseras*[a,c]

Received 12th February 2009, Accepted 29th May 2009
First published as an Advance Article on the web 22nd June 2009
DOI: 10.1039/b902947h

The spontaneous oxidation of an amine group to an imine has been observed experimentally in an octa-aza macrocyclic dinucleating ligand LH_4 coordinated to Cu^{II}. The reaction is bimolecular and spontaneous in which amine groups of one macrocycle are oxidised and the Cu^{II} centres of a second macrocyclic complex are reduced. No additional oxidating or external base agents are required. DFT calculations are carried out to compare the reaction with that recently reported for a ligand coordinated to an Fe^{III} centre, but which requires an external base as proton acceptor. The computational results show that the copper and iron catalysed amine to imine reactions proceed *via* different mechanisms.

Introduction

Amine oxidative dehydrogenation is widespread in biochemistry. Amine oxidases are found in bacteria, yeast, plants and mammals, and are involved in important biological processes, including lysyl oxidation in crosslinking of collagen and the regulation of neurotransmitters such as dopamine and serotonin.[1–4] The family of amine oxidases includes flavoproteins and quinoproteins, a subset of which are the copper containing amine oxidases.[4,5] However many of the mechanistic details are still unknown.

Amine oxidation in synthetic macrocycles bound to transition metals was first discovered by Curtis for four coordinate Ni^{II} complexes where nitric acid acts as the oxidising agent.[6] Since then amine oxidation has been observed for many transition metals, the most common including Ru, Fe, Ni, Cu, and Os.[7,8] The reactivity is observed for a range of ligands from bi- and mono-dentate ligands, up to the six-coordinate cage ligand in the $[Ru(sar)]^{2+}$ complex, where sar = sarcophagine, 3,6,10,13,16,19-hexaazabicyclo[6.6.6]eicosane. For this complex all six amine donors are oxidised to imines.[9] The reactivity of complexes towards amine oxidation is sensitive to the nature of the ligand and to the identity of the metal. For example for the macrocyclic systems initially studied by Curtis, Fe was shown to be able to undergo the same reaction with a milder oxidising agent,[7,10,11] while Cu^{II} and Ni^{II} required more strongly oxidising conditions.[12] In contrast, Co^{III} was found to be inactive. More recently, Ru and Os have been shown to be especially effective at oxidating coordinated amines and alcohols, which has been attributed to their ability to access oxidation states two higher than the final state.[7,13,14]

Amine to imine oxidation has been recently studied for a macrocyclic $[Fe^{III}H_2L^2]^{3+}$ complex, H_2L^2 = 1,9-bis(2′pyridyl)-5-[(ethoxy-2”-pyridyl)methyl]-2,5,8-triazanonane.[14,15] In this reaction, one of the ligand amine donors is oxidised and the metal is reduced, leading to the formation of a stable Fe^{II} complex which has been isolated and characterized by X-ray crystallography.[15] The general themes of this mechanism are common to several amine to imine oxidations, including those proposed for the $[Ru(bpy)_2(ampy)]^{2+}$ complex,[7,16] and a series of $[Fe^{III}(CN)_4(1,2\text{-diamine})]^{+}$ complexes.[8] The $[Fe^{III}H_2L^2]^{3+}$ reaction is novel in that it occurs spontaneously in the absence of an external oxidant, however the general mechanism is representative of the behaviour of many systems of this type, in that it involves elementary proton and electron transfer steps.

In this study, we present a copper catalysed amine to imine reaction in a macrocyclic complex, $[Cu^{II}_2(H_4L)]^{4+}$, where L is the octaazamacrocyclic dinucleating ligand shown in Scheme 1. This complex is part of a family of binuclear copper complexes, which show interesting reactivity towards molecular O_2.[17–22] This amine

[a]*Institute of Chemical Research of Catalonia (ICIQ), Avgda. Països Catalans 16, 43007 Tarragona, Catalonia, Spain. E-mail: fmaseras@iciq.es, allobet@iciq.es; Fax: +34 977920231; Tel: +34 977920202*
[b]*Departament de Química, Universitat de Girona, Campus de Montilivi 17071 Girona, Spain. E-mail: angeles.martinez@udg.edu*
[c]*Departament de Quimica, Universitat Autonoma de Barcelona, 08193 Bellaterra, Catalonia, Spain*

† Electronic supplementary information (ESI) available: Cartesian coordinates for computed geometries and selected bond lengths and angles for Fe and Cu imine complexes. CCDC reference numbers 720266 and 720267. For ESI and crystallographic data in CIF or other electronic format see DOI: 10.1039/b902947h

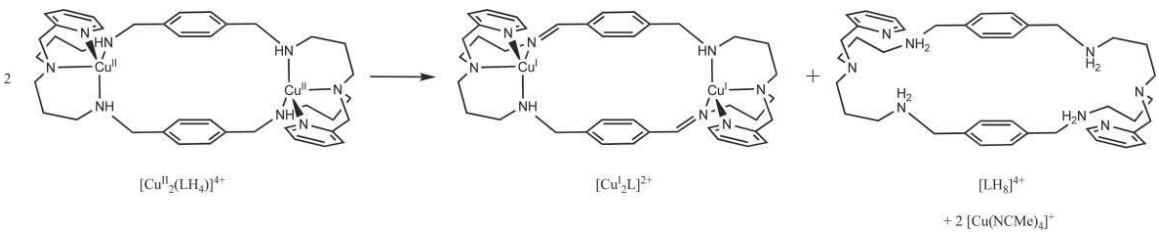

Scheme 1 The copper catalysed amine to imine reaction (reaction 2).

oxidation reaction, like the iron system mentioned above, does not require an external oxidant, and represents a further advance in that it does not require addition of base. Given the similarities in the chemistry between the systems, the amine to imine mechanism proposed for $[Fe^{III}H_2L^2]^{3+}$ is studied computationally for both the $[Fe^{III}H_2L^2]^{3+}$ and $[Cu^{II}{}_2(H_4L)]^{4+}$ systems.

Experimental

Physical methods

The ESI-MS experiments were performed on a Navigator LC/MS chromatograph from Thermo Quest Finigan, using acetonitrile as the mobile phase.

Materials and synthesis

Reagents and solvents used were of commercially available reagent quality unless otherwise stated. Solvents were purchased from SDS. The ligand LH_4 was obtained according to literature procedures.[23]

Synthesis of $[Cu_2(L)](CF_3SO_3)_2$ and $(LH_8)(CF_3SO_3)_4$

To a suspension of LH_4 (0.036 g, 0.055 mmol) in 1 mL of MeCN under magnetic stirring was added 2 mL of another MeCN solution containing 0.040 g (0.110 mmol) of $Cu(CF_3SO_3)_2$. The solution was stirred for one hour at room temperature and then allowed to diffuse under a saturated solution of diethyl ether for a week also at room temperature. After this time, white and orange crystals appeared that correspond to the compounds $(LH_8)(CF_3SO_3)_4$ and $[Cu_2(L)](CF_3SO_3)_2$, respectively.

X-Ray structure determination

$[LH_8](CF_3SO_3)_4$. A white crystal was mounted on a nylon loop and used for low temperature (100(2) K) X-ray structure determination. The measurement was carried out on a BRUKER SMART APEX CCD diffractometer using graphite-monochromated Mo Kα radiation ($\lambda = 0.71073$ Å). The measurements were made in the range 2.20–28.36° for θ. Full-sphere data collection was carried out with ω and φ scans. A total of 23 583 reflections were collected of which 7433 [$R_{int} = 0.0503$] were unique. Programs used: data collection, Smart version 5.631 (Bruker AXS 1997–02); data reduction, Saint+ version 6.36A (Bruker AXS 2001); absorption correction, SADABS version 2.10 (Bruker AXS 2001).[24] Structure solution and refinement was done using SHELXTL Version 6.14 (Bruker AXS 2000–2003).[24] The structure was solved by direct methods and refined by full-matrix least-squares methods on F^2. Large voids containing residual electron density peaks are found in the structure. No solvent molecules could be identified to match the spurious density, so the peaks were removed from the observed data with The SQUEEZE tool from PLATON.[25]

The non-hydrogen atoms were refined anisotropically. The H-atoms were placed in geometrically optimized positions and forced to ride on the atom to which they are attached, except the amino hydrogens that were placed in the difference Fourier map. The N1–H1 distance was constrained to 0.87(1) Å, and the rest of the amino hydrogens were refined without constrains. The asymmetric unit contains half macrocycle and two $CF_3SO_3^-$ counterions.

$[Cu_2(L)](CF_3SO_3)_2 0.5Et_2O{\cdot}MeCN{\cdot}0.4H_2O$. An orange crystal was mounted on a nylon loop and used for low temperature (100(2) K) X-ray structure determination. The measurement was carried out on a BRUKER SMART APEX CCD diffractometer using graphite-monochromated Mo Kα radiation ($\lambda = 0.71073$ Å). The measurements were made in the range 2.08–28.31° for θ. Full-sphere data collection was carried out with ω and φ scans. A total of 78 188 reflections were collected of which 12 726 [$R_{int} = 0.0299$] were unique. Programs used: data collection, Smart version 5.631 (Bruker AXS 1997–02); data reduction, Saint+ version 6.36A (Bruker AXS 2001); absorption correction, SADABS version 2.10 (Bruker AXS 2001).[24] Structure solution and refinement was done using SHELXTL version 6.14 (Bruker AXS 2000–2003).[24] The structure was solved by direct methods and refined by full-matrix least-squares methods on F^2.

A considerable amount of electron density attributable to a partially disordered di-ethyl ether solvent molecule and a H_2O solvent molecule was removed with the SQUEEZE option of PLATON.[25] Those solvent molecules are, however, included in the reported chemical formula and derived values (*e.g.* formula weight, *F*_000, *etc.*).

The non-hydrogen atoms were refined anisotropically. All the H-atoms were placed in geometrically optimized positions and forced to ride on the atom to which they are attached except the imine hydrogens which were found in the difference map and refined without constrains.

Computational details

Density functional theory calculations were performed using the Gaussian 03 suite of programs,[26] with the B3LYP* functional.[27] This functional differs from the commonly used B3LYP functional.[28,29] in that it has 15% instead of 20% exact exchange and often better reproduces spin-state splittings in transition metal complexes.[30] The structures were optimized using the SDD basis set[31] for Cu, Fe, S and Cl while the 6–31G(d)[32,33] basis set was used for all remaining atoms. Solvent effects for the model system were calculated using single-point PCM[34] calculations on gas phase geometries with acetonitrile as the solvent for the copper system and ethanol for the iron system. In both cases UFF radii were used for the construction of the cavity. The solvation model explicitly includes solute hydrogen atoms in the cavity construction. Minima were confirmed through frequency calculations and reported energies include zero-point energy corrections.

For the $[Cu^{II}{}_2(H_4L)]^{4+}$ system, calculations were carried out on a mononuclear model system with one Cu centre, as shown in Fig. 1. This model retains the ligand coordination of the real system. For $[Fe^{III}L^2]^{3+}$, the system was modelled as shown in Fig. 1, which differs from the experimental system only in the absence of the ethoxy side arm and the replacement of the BPh_4^- counterions by chloride. Where explicit solvent molecules were included in the calculations, the experimental acetonitrile was used for the copper system, while ethanol was replaced by methanol in the iron system. The coordination energies of ethanol and methanol to Fe^{II} differ by less than 1 kJ mol^{-1}.

The importance of the counterion and solvent molecules was tested for each complex studied, and were included where they

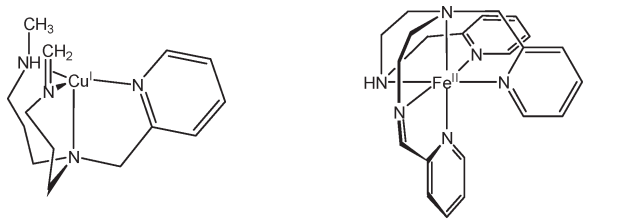

Fig. 1 Computational models of (A) $[Cu^{I}_{2}(L)]^{2+}$ and (B) $[Fe^{II}L]^{2+}$ complexes.

were found to be coordinating or to have a significant effect on the relative energy of the complexes.

Results and discussion

Synthesis, structure and characterization

The octaazamacrocyclic dinucleating ligand LH_4 reacts rapidly in acetonitrile with Cu^{II} salts to form a deep blue complex as indicated in the following reaction,

$$LH_4 + 2Cu^{II} \rightarrow [Cu^{II}_{2}(LH_4)]^{4+} \quad (1)$$

This blue Cu^{II} complex slowly suffers an internal redox reaction (see Scheme 1) that leads to the partial oxidation of the amine groups of the LH_4 ligand and reduction of the metal center.

This generates an orange Cu^{I} complex, $[Cu^{I}_{2}L]^{2+}$, while the original ligand becomes tetraprotonated, LH_8^{4+}, and the remaining Cu^{I} is coordinated by 4 solvent molecules, $[Cu^{I}(NCMe)_4]^{+}$. It is important to outline here that this reaction proceeds both in the absence of an external oxidant and an external base. The latter function is carried out by the original ligand where the four secondary amines become protonated.

Sufficiently good crystals of $[Cu^{I}_{2}L]^{2+}$ and LH_8^{4+} were obtained for a monocrystal X-ray analysis and their main crystallographic data are reported in Tables 1 and 2. Furthermore, an ORTEP view of their cationic parts are displayed in Fig. 2. In both cases, bond distances and angles are within the normal values obtained for these type of compounds.[17–19,21,22,35–37] For the $[Cu^{I}_{2}L]^{2+}$ complex, each Cu metal center adopts a distorted tetrahedral geometry due to the constraints imposed by the coordinating N atoms of the macrocyclic ligand. The central tertiary amine N has the largest distance, 2.345 Å, whereas the secondary amine N and the pyridylic N at situated at similar distances, 2.23 and 2.22 Å respectively. Finally, the iminic N has the shortest bond distance at 1.98 Å. It is interesting to realize here the uniqueness of this complex from a coordination point of view, since the 4 N atoms that coordinate to the Cu center have a different chemical nature and as a consequence each Cu atom becomes a chiral center. The two Cu atoms are situated at 7.677 Å apart as a consequence of the *para* substitution and thus prevent any direct metal–metal interaction. The Cu centers are related by a pseudo C_2 axis of symmetry that is situated in between and parallel to the two phenyl rings which are nearly parallel to one another (the angle between rings is 13.06°). On the other hand the pyridyl rings are rotated by 33.36°. With regard to one another. The nature of the C=N sp^2 iminic bond is corroborated by the C–N bond distances that are 0.3 Å shorter than that of a typical sp^3 C–N aminic bond of the starting ligand.

Table 1 Crystallographic data for the tetraprotonated ligand $(LH_8)(CF_3SO_3)_4$ and for the mixed imine-amine complex $[Cu_2(L)](CF_3SO_3)_2$

Complex	$[Cu_2(L)](CF_3SO_3)_2$ $0.5Et_2O{\cdot}MeCN{\cdot}0.39H_2O$	$(LH_8)(CF_3SO_3)_4$
Empirical formula	$C_{46}H_{62}Cu_2F_6N_9O_{7.5}S_2$	$C_{44}H_{60}F_{12}N_8O_{12}S_4$
Molecular mass/g mol^{-1}	1166.25	1249.24
T/K	100(2)	100(2)
Crystal system, space group	Monoclinic, $P2_1/c$	Triclinic, $P\bar{1}$
a/Å	12.413(6)	8.943(6)
b/Å	19.459(9)	11.522(7)
c/Å	21.578(10)	15.737(10)
α/°	90	86.055(11)
β/°	97.086(8)	86.660(11)
γ/°	90	73.590(11)
V/Å^3	5172(4)	1550.6(17)
Z	4	1
ρ/g cm^{-3}	1.498	1.338
$R\,[I > 2\sigma(I)]^a$	0.0333	0.0612
w$R\,[I > 2\sigma(I)]$	0.0903	0.1646

^{a} $R = \sum[F_o - F_c]/\sum F_o$; w$R = [\sum(w(F_o^2 - F_c^2)^2/\sum(wF_o^4)]^{1/2}$.

Table 2 Metric parameters (in Å and °) for the cationic part of complex $[Cu_2(L)](CF_3SO_3)_2$

Distances/Å			
Cu1–N1	1.975	Cu2–N5	1.984
Cu1–N2	2.203	Cu2–N6	2.212
Cu1–N3	2.050	Cu2–N7	2.058
Cu1–N4	2.046	Cu2–N8	2.058
Cu1–Cu2	7.677		
Bond angles/°			
N1–Cu1–N2	101.71	N5–Cu2–N6	101.76
N2–Cu1–N4	100.47	N6–Cu2–N8	99.13
N2–Cu1–N3	81.15	N6–Cu2–N7	81.45
N3–Cu1–N1	129.49	N7–Cu2–N5	127.49
N3–Cu1–N4	111.49	N7–Cu2–N8	109.67
N1–Cu1–N4	117.27	N5–Cu2–N8	121.12

Comparison with the iron system

There are intriguing similarities between the amine to imine reaction carried out by the Cu complex presented here and the iron system, $[Fe^{III}H_2L^2]^{3+}$, where H_2L^2 = 1,9-bis(2′pyridyl)-5-[(ethoxy-2″-pyridyl)methyl]-2,5,8-triazanonane, studied by Sosa-Torres and co-workers.[14,15] The reaction for the copper system, presented above is:

$$2[Cu^{II}_{2}(LH_4)]^{4+} + 8MeCN \rightarrow [Cu^{I}_{2}L]^{2+} + [LH_8]^{4+} + 2[Cu^{I}(NCMe)_4]^{+} \quad (2)$$

For the iron catalysed amine to imine reaction in $[Fe^{III}H_2L^2]^{3+}$ the reaction is[15]:

$$2[Fe^{III}H_2L^2]^{3+} + 2EtO^- \rightarrow [Fe^{II}H_2L^2]^{2+} + [Fe^{II}L^2]^{2+} + 2EtOH \quad (3)$$

In both cases, there is an original reactant complex with the metal in a high oxidation state and a secondary amine ligand. This reactant evolves to two different product complexes. In both

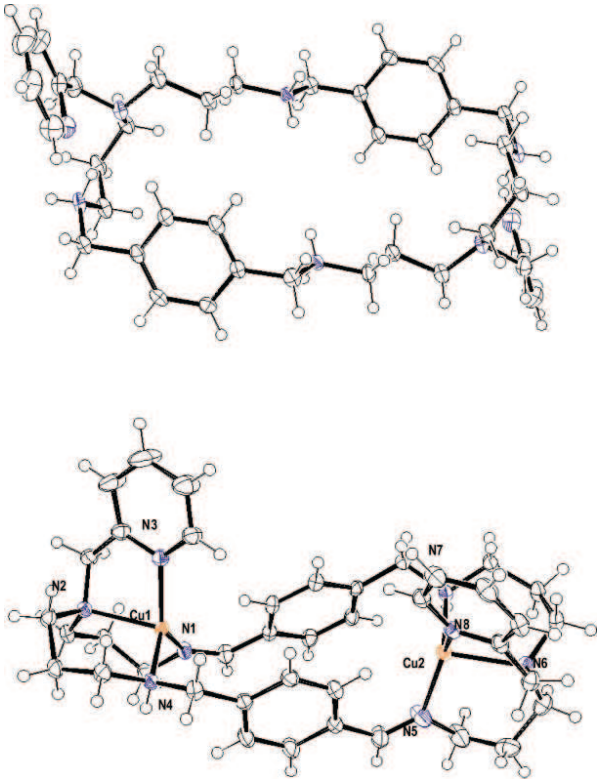

Fig. 2 Top, ORTEP plot (50% probability) for the cationic side of the tetraprotonated dinucleating macrocyclic ligand LH_8. Bottom, ORTEP plot (50% probability) for the mixed imine-amine dinuclear Cu complex with labels for key atoms.

of them the metal has reduced the oxidation state by one. One of the two product complexes contains an imine ligand, resulting from the formal oxidation by two electrons of the original amine ligand. No external oxidant is required for either system.

There are two key formal differences between the two systems. The first of them is the dinuclear character of the copper complexes with the macrocycle. This can be however easily handled if we replace the large ligand by the model ligand H_2L' shown in Fig. 1. By doing this, reaction (2) becomes reaction (2m), m standing for model:

$$2[Cu^{II}(H_2L')]^{2+} + 4MeCN \rightarrow [Cu^{I}L']^{+} + [H_4L']^{2+} + [Cu^{I}(NCMe)_4]^{+} \quad (2m)$$

This model retains the ligand coordination at the metal centre of the real system, and only differs from the experimental system in the absence of the linkers and second copper centre.

The use of a mononuclear model can be justified as the two copper centres in the experimental system are not expected to interact to any significant degree as they are separated by over 7 Å with a relatively rigid linker between them. It is difficult to envisage how these two centres could "talk" to each other, and it seems more likely that the reaction is bimolecular, with two different complexes involved. Because of this, the separation of the dimer in two model monomers seems justified.

The second difference, which seems to carry more chemical relevance, is the nature of the proton acceptor or base. In the case of iron, the reaction is pH dependent and shows base catalysis. In contrast, in the copper system the ligand of a second macrocycle accepts the protons and no additional base is required to drive the reaction. This is highlighted in Scheme 2, which summarises the important aspects of the overall reactions. The mechanisms have been labelled as external and internal proton acceptor pathways.

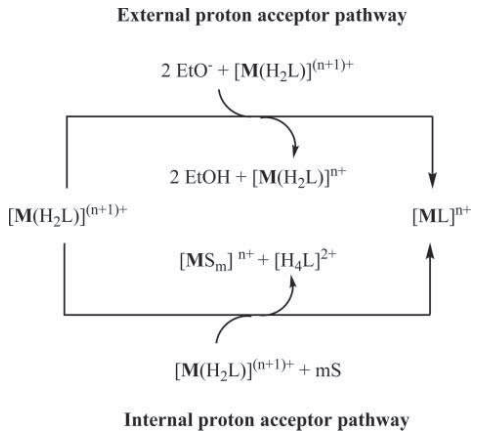

Scheme 2 External and internal proton acceptor pathways for amine to imine oxidation for the Cu and Fe systems. For M = Fe $n = 2$, $m = 6$ and S = MeOH. For M = Cu $n = 1$, $m = 4$ and S = NCMe.

Kinetic studies of the iron reaction, and the observation of a second Fe^{II} complex present in the reaction have lead to the proposal in Scheme 3,[15] for the mechanism of the external proton acceptor (EPA) pathway. The mechanism has three steps: (a) first deprotonation, (b) electron transfer between the two complexes, (c) second deprotonation. The internal proton acceptor pathway (IPA) is first reported here, and thus no previous mechanistic proposal is available. In this study, DFT calculations are used to determine whether the reaction is able to proceed *via* a mechanism similar to the EPA reaction. To this end, both IPA and EPA mechanisms are explored computationally for both the iron and copper systems. Optimised geometries for the iron and copper complexes are shown in Fig. 3, and selected bond lengths are tabulated in Table 3. Calculated reaction energies are included in Table 4.

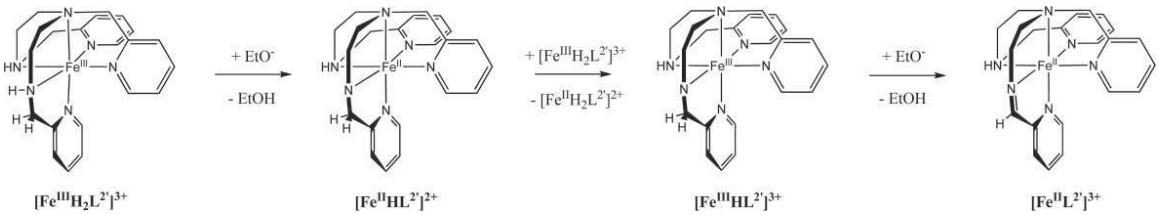

Scheme 3 Proposed reaction mechanism for $[Fe^{III}H_2L^{2'}]^{3+}$.

Table 3 Selected calculated bond lengths (Å) with corresponding experimental values in parentheses where available

	Reactant	Product 1	Product 2
Bond	$[Cu^{II}(H_2L')][CF_3SO_3]_2$	$[Cu^{I}(L')]$	$[Cu^{I}(H_4L')][CF_3SO_3]$
N_1–C_1	1.483	1.281 (1.277/1.288)	1.487
Cu–N_1	2.066	1.996 (1.984/1.975)	4.205
Cu–N_2	2.327	2.247 (2.211/2.204)	2.476
Cu–N_3	2.102	2.066 (2.058/2.051)	1.969
Cu–N_4	2.046	2.093 (2.058/2.046)	5.493
Cu–O_1	2.119	—	2.033
Cu–O_2	4.177	—	2.067
Cu–O_3	—	—	4.708

Bond	Reactant $[Fe^{III}H_2L^{2'}]Cl_3$	Product 1 $[Fe^{II}L^{2'}]Cl_2$[a]	Product 2 $[Fe^{II}H_2L^{2'}]Cl_2$
Fe–N_1	2.002	2.006 (1.946)	2.009
Fe–N_2	1.937	1.918 (1.853)	1.995
Fe–N_3	2.038	2.052 (2.007)	2.046
Fe–N_4	1.988	2.005 (1.942)	2.021
Fe–N_5	2.020	2.063 (2.007)	2.069
Fe–N_6	2.066	2.038 (1.977)	2.031
N_2–C_1	1.484	1.294 (1.269)	1.481
Fe–Cl_1	4.211	4.240	4.288
Fe–Cl_2	4.395	4.435	4.497
Fe–Cl_3	4.451	—	—

[a] Experimental values from Sosa-Torres and co-workers.[38]

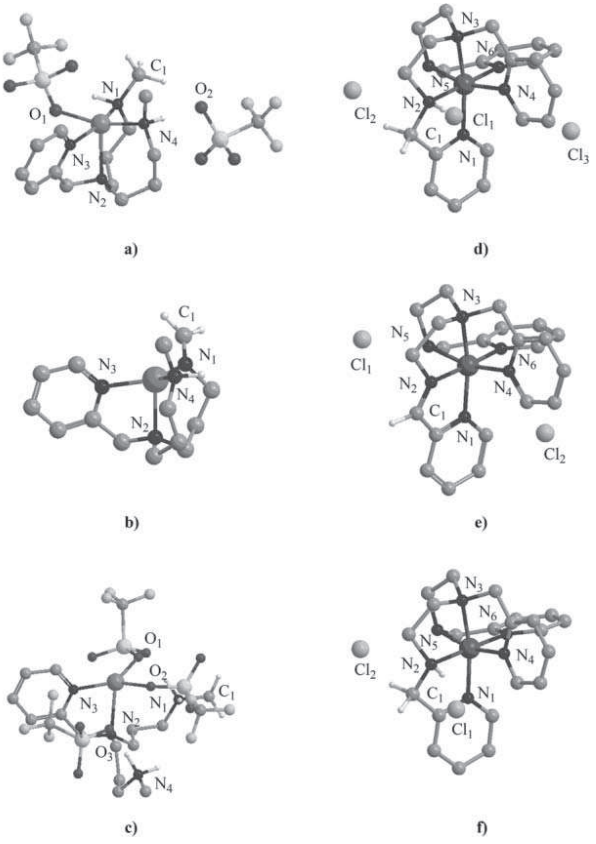

Fig. 3 Optimised structures for the Cu and Fe systems. (a) $[Cu^{II}(H_2L')][CF_3SO_3]_2$ (b) $[Cu^{I}(L')]$, (c) $[Cu^{I}(H_4L')][CF_3SO_3]_2$, (d) $[Fe^{III}H_2L^{2'}]Cl_3$, (e) $[Fe^{II}L^{2'}]Cl_2$ and (f) $[Fe^{II}H_2L^{2'}]Cl_2$. Hydrogen atoms which participate in the reaction are shown. These include all hydrogens bound to nitrogen atoms and those bound to C_1, atoms.

Computed geometries

Three complexes are reported for each system, the reactant, containing the oxidated metal and the reduced ligand; and the two products, one with the reduced metal and the oxidated ligand (labelled as product 1), and the other with the reduced metal and the reduced ligand (product 2).

For the copper system the reactant, $[Cu^{II}(H_2L')][CF_3SO_3]_2$, is calculated to have an approximately square-pyramidal five-coordinate geometry with the amine donor, N_3, at the apex, and one of the triflate counter-ions completing the coordination sphere. The second counter-ion is non-coordinating (Cu–O = 4.177 Å). Coordination of a triflate counter-ion to the copper centre in Cu^{I} complexes of this family has been observed previously.[17]

The $[Cu^{I}L']$ product is calculated to have trigonal pyramidal geometry with bond lengths in good agreement with the experimental structure. When included, the counter-ion has a very small effect on the energy (binding energy of only 8 kJ mol^{-1}) but distorts unrealistically the Cu coordination sphere by exerting a *trans* influence on one of the Cu–N bonds.

For the second product complex, $[Cu^{I}(H_4L')][CF_3SO_3]_2$, the calculated structure shows that upon protonation the N_1 and N_4 ligand donors dissociate from the metal centre. In the absence of solvent molecules in the model their place is taken by two counter-ions to give structure (c) in Fig. 3. However, acetonitrile binds more strongly to the metal centre and, when included, displaces the counter-ions. This is accompanied by a lengthening and then breaking of the Cu–N_2 bond, and eventual dissociation of the ligand from the metal centre to form $[H_4L'][CF_3SO_3]_2$ and $[Cu^{I}(NCMe)_4][CF_3SO_3]$.

For the iron system, all complexes are calculated to have approximately octahedral coordination around the metal centres, with N–Fe–N bond angles ranging between 81 and 99° for the

Table 4 Calculated potential energies of reaction for the $[Fe^{III}H_2L^{2'}]^{3+}$ and $[Cu^{II}(H_2L')]^{2+}$ systems. In all reactions counter-ions are included to counter the charges of the metal complexes and free ligands

	ΔE/kJ mol^{-1}	
	M = Fe	M = Cu
External proton acceptor (EPA) pathway[a]		
$2[M(H_2L)]^{(n+1)+} + 2EtO^- \rightarrow [ML]^{n+} + [M(H_2L)]^{n+} + 2EtOH$	−433.0	−109.2
EPA (a) $[M(H_2L)]^{(n+1)+} + [EtO^-] \leftrightarrow [M(HL)]^{n+} + [EtOH]$	−149.5	−79.4
EPA (b) $[M(HL)]^{n+} + [M(H_2L)]^{(n+1)+} \rightarrow [M(HL)]^{(n+1)+} + [M(H_2L)]^{n+}$	+79.7	+243.8
EPA (c) $[M(HL)]^{(n+1)+} + [EtO^-] \rightarrow [ML]^{n+} + [EtOH]$	−363.3	−273.6
Internal proton acceptor (IPA) pathway[b]		
$2[M(H_2L)]^{(n+1)+} + mS \rightarrow [ML]^{n+} + [H_4L]^{2+} + [MS_m]^{n+}$	−107.1	−7.24

[a] $n = 2$ and 1 for M = Fe and Cu, respectively. [b] $m = 6$, S = MeOH for Fe. For Cu $m = 4$, S = NCMe.

$[Fe^{II}L^{2'}]Cl_2$ product. This broad range is also observed in the crystal structure for this species and calculated bond angles are within 2.5° of the experimental values (see ESI).† Again, as in the case for the copper complex, the metal–N bond lengths show a lengthening compared to experiment.

Unlike the copper system, the structural differences between the iron complexes are not large, as there is no change in coordination number or the geometry at the Fe centre. In this system the counterion is non-bonding maintaining Fe–Cl distances of greater than 4.2 Å. There is a general lengthening of the Fe–N bonds in the products, with the exception of the Fe–N_2 bond in $[Fe^{II}L^{2'}]Cl_2$, which shortens on deprotonation of N_2 and formation of the N_2–C_1 double bond.

Computed energies

The overall energies for the external proton acceptor (EPA) reaction, which is the reaction observed experimentally for iron, and the internal proton acceptor (IPA) reaction, which is observed for copper, were calculated for both the copper $[Cu^{II}(H_2L')]^{2+}$ and the iron $[Fe^{III}H_2L^{2'}]$ systems.

The EPA reaction can be further broken down into the individual steps (first deprotonation, electron transfer, second deprotonation) shown in Scheme 3 for the iron system:

$$[M(H_2L)]^{(n+1)+} + [EtO^-] \leftrightarrow [M(HL)]^{n+} + [EtOH] \quad \text{(EPA a)}$$

$$[M(HL)]^{n+} + [M(H_2L)]^{(n+1)+} \rightarrow [M(HL)]^{(n+1)+} + [M(H_2L)]^{n+} \quad \text{(EPA b)}$$

$$[M(HL)]^{(n+1)+} + [EtO^-] \rightarrow [ML]^{n+} + [EtOH] \quad \text{(EPA c)}$$

The energy for each reaction step was calculated for M = Fe^{III} and Cu^{II} and the values are included in Table 4.

The overall EPA reaction is calculated to be strongly exothermic for iron, at −433 kJ mol^{-1}. The calculated energies for reaction steps EPA (a), EPA (b) and EPA (c) show that this can be attributed to the deprotonation steps which are exothermic by 149.5 and 363.3 kJ mol^{-1}, respectively. In comparison, the electron transfer step is calculated to be endothermic by 80 kJ mol^{-1}. The strong exothermicity of the deprotonation steps can be shown to be due to the nature of the base, EtO^-, as deprotonation step EPA (a) is predicted to be endothermic by 186 kJ mol^{-1} when H_2O replaces EtO^- as the base.

The EPA reaction for the copper system was found to be also exothermic, albeit by a smaller amount of 109 kJ mol^{-1}. The lower exothermicity can be easily explained by the redox potentials for the two metals of 0.771 and 0.153 for Fe^{III}/Fe^{II} and Cu^{II}/Cu^{I}, respectively,[39] and the different charges of the starting complexes. These charges have a key effect on the acidity of the compound, which is obviously a key factor in any proton transfer process. However, the fact that the reaction remains exothermic indicates that this mechanism could still be operative for the copper system. An analysis of the reaction steps, also in Table 4, proves that this is not the case. The electron transfer step (b) is strongly endothermic for the copper system, with a value of +244 kJ mol^{-1}. Therefore, although thermodynamically favourable, the EPA reaction is kinetically unfavourable and only the deprotonated complex, $[Cu^{II}(HL')]^+$ is predicted to form in the presence of base.

The internal proton acceptor (IPA) reaction, that observed experimentally for copper, was also studied for both the copper and iron complexes. In comparison to the EPA reaction, it is calculated to be significantly less favourable with predicted exothermicities of 7 kJ mol^{-1} and 107 kJ mol^{-1}, for copper and iron respectively. The difference in exothermicity between these reactions is not unexpected given that protonation of ethoxide provides a large part of the driving force for the EPA reaction.

The IPA pathway is calculated to be thermodynamically favourable for both systems. The inability of the more oxidising iron system to carry out the reaction in the absence of base thus makes the experimental copper reaction even more intriguing and it seems clear that despite the formal similarities, the reaction mechanisms are substantially different. Full characterization of the mechanism for the copper system requires more detailed studies that are beyond the scope of this work.

Characterization of the IPA mechanism will hopefully clarify why it is not operative for the iron system. Even without a complete understanding of the mechanism, one important difference between the two systems which can be identified, and which favours the IPA reaction in the copper system, is the dissociation of the ligand and replacement by solvent molecules. The energy of dissociation of the ligand, H_2L, from the reduced metal centre and

replacement by solvent (reaction 4 shown below) was calculated for both copper and iron, where S = MeOH with $m = 6$ for iron, and S = NCME and $m = 4$ for copper.

$$[M(H_2L)]^{n+} + mS \rightarrow [MS_m]^{n+} + H_2L \quad (4)$$

Replacement of the H_2L ligand by acetonitrile was calculated to be strongly exothermic for copper at 144 kJ mol^{-1}, which is consistent with the known affinity of acetonitrile for Cu^{I}.[40] In comparison, the corresponding reaction for iron was calculated to be only very weakly exothermic at 9 kJ mol^{-1}. This difference in the coordinating ability of the solvent leads to the stabilisation of the copper products in the IPA reaction compared to those of iron. Based on this result, we predict that the reaction would be blocked for the copper system if it were carried out in a weakly coordinating solvent.

Conclusions

The copper catalysed oxidation of a coordinated amine to an amine has been reported for $[Cu^{II}_2(LH_4)]^{4+}$. The reaction is bimolecular in which the amine groups of one macrocycle are oxidised to an imine and the Cu^{II} centres and the second macrocycle are reduced. The reaction proceeds both in the absence of an external oxidant and an external base. Instead the original ligand carries out the role of the base where the four secondary amines become protonated.

The amine to imine reaction was explored computationally for the copper complex and for a $[Fe^{III}H_2L^2]^{3+}$ complex which undergoes a similar amine oxidation, also in the absence of external oxidant. The iron catalysed reaction is calculated to be exothermic and was found to be driven by the protonation of the base, ethoxide. The reaction in the presence of base was also calculated to be exothermic for copper, however the key electron transfer step is calculated to be strongly endothermic, and hence the reaction is predicted to be unfavourable on kinetic grounds.

The experimentally observed copper catalysed reaction was also calculated to be favourable for both systems. The coordination of the solvent to the Cu^{I} centre after ligand dissociation was found to be important for stabilising the products. Without this additional stabilisation the reaction is expected to be significantly endothermic, and we predict that the reaction would not be observed for copper in the presence of a less coordinating solvent. Full characterization of the mechanism for the copper mechanism is currently the subject of research in our laboratory.

Acknowledgements

We gratefully acknowledge the Spanish MICINN (Consolider Ingenio 2010, Grant CSD 2006-0003) and the ICIQ Foundation for financial support.

This research has been financed by MEC of Spain through project CTQ2007-67918-C03-03/BQU. A. A. is grateful for the award of a doctoral grant from CIRIT Generalitat de Catalunya.

References

1 C. Binda, A. Mattevi and D. E. Edmondson, *J. Biol. Chem.*, 2002, **277**, 23973–23976.
2 N. S. Scrutton, *Natl. Prod. Rep.*, 2004, **21**, 722–730.
3 D. E. Edmondson, C. Binda and A. Mattevi, *Arch. Biochem. Biophys.*, 2007, **464**, 269–276.
4 J. P. Klinman, *Chem. Rev.*, 1996, **96**, 2541–2562.
5 I. S. MacPherson and M. E. P. Murphy, *Cell. Mol. Life Sci.*, 2007, **64**, 2887–2899.
6 N. F. Curtis, Y. M. Curtis and H. K. J. Powell, *J. Chem. Soc. A*, 1966, 1015–1018.
7 F. R. Keene, *Coord. Chem. Rev.*, 1999, **187**, 121–149.
8 M. Goto, M. Takeshita, N. Kanda, T. Sakai and V. L. Goedken, *Inorg. Chem.*, 1985, **24**, 582–587.
9 P. Bernhard and A. M. Sargeson, *J. Am. Chem. Soc.*, 1989, **111**, 597–606.
10 V. L. Goedken and D. H. Busch, *J. Am. Chem. Soc.*, 1972, **94**, 7355–7363.
11 C. J. Hipp, L. F. Lindoy and D. H. Busch, *Inorg. Chem.*, 1972, **11**, 1988–1994.
12 D. C. Olson and J. Vasilevskis, *Inorg. Chem.*, 1971, **10**, 463–470.
13 F. R. Keene, M. J. Ridd and M. R. Snow, *J. Am. Chem. Soc.*, 1983, **105**, 7075–7081.
14 V. M. Ugalde-Saldívar, M. E. Sosa-Torres, L. Ortiz-Frade, S. Bernès and H. Höpfl, *J. Chem. Soc., Dalton Trans.*, 2001, 3099–3107.
15 J. P. Saucedo-Vázquez, V. M. Ugalde-Saldívar, A. R. Toscano, P. M. H. Kroneck and M. E. Sosa-Torres, *Inorg. Chem.*, 2009, **48**, 1214–1222.
16 M. J. Ridd and F. R. Keene, *J. Am. Chem. Soc.*, 1981, **103**, 5733–5740.
17 A. Company, L. Gomez, R. Mas-Balleste, I. V. Korendovych, X. Ribas, A. Poater, T. Parella, X. Fontrodona, J. Benet-Buchholz, M. Sola, L. Que, E. V. Rybak-Akimova and M. Costas, *Inorg. Chem.*, 2007, **46**, 4997–5012.
18 A. Company, J. E. Jee, X. Ribas, J. M. Lopez-Valbuena, L. Gomez, M. Corbella, A. Llobet, J. Mahia, J. Benet-Buchholz, M. Costas and R. van Eldik, *Inorg. Chem.*, 2007, **46**, 9098–9110.
19 A. Company, D. Lamata, A. Poater, M. Sola, E. V. Rybak-Akimova, L. Que, X. Fontrodona, T. Parella, A. Llobet and M. Costas, *Inorg. Chem.*, 2006, **45**, 5239–5241.
20 M. Costas, C. Anda, A. Llobet, T. Parella, H. S. Evans and E. Pinilla, *Eur. J. Inorg. Chem.*, 2004, 857–865.
21 M. Costas, X. Ribas, A. Poater, J. M. L. Valbuena, R. Xifra, A. Company, M. Duran, M. Sola, A. Llobet, M. Corbella, M. A. Uson, J. Mahia, X. Solans, X. P. Shan and J. Benet-Buchholz, *Inorg. Chem.*, 2006, **45**, 3569–3581.
22 M. Costas, R. Xifra, A. Llobet, M. Sola, J. Robles, T. Parella, H. Stoeckli-Evans and M. Neuburger, *Inorg. Chem.*, 2003, **42**, 4456–4468.
23 A. Arbuse, M. A. Martinez and A. Llobet, *manuscript in preparation*.
24 Bruker Advanced X-ray Solutions. SMART: Version 5.631, 1997–2002; Bruker Advanced X-ray Solutions. SAINT+, Version 6.36A, 2001; G. M. Sheldrick, Program for Crystal Structure Refinement, Universität Göttingen, 1997 Bruker Advanced X-ray Solutions. SHELXTL Version 6.14, 2000-2003; G. M. Sheldrick, Empirical Absorption Correction Program, Universität Göttingen, 1996, Bruker Advanced X-ray Solutions. SADABS Version 2.10, 2001.
25 (*a*) A. L. Spek, *J. Appl. Crystallogr.*, 2003, **36**, 7–13; (*b*) A. L. Spek, *PLATON, A Multipurpose Crystallographic Tool*, Utrecht University, Utrecht, The Netherlands, 2005.
26 M. J. Frisch, G. W. Trucks, H. B. Schlegel, G. E. Scuseria, M. A. Robb, J. R. Cheeseman, J. A. Montgomery, Jr., T. Vreven, K. N. Kudin, J. C. Burant, J. M. Millam, S. S. Iyengar, J. Tomasi, V. Barone, B. Mennucci, M. Cossi, G. Scalmani, N. Rega, G. A. Petersson, H. Nakatsuji, M. Hada, M. Ehara, K. Toyota, R. Fukuda, J. Hasegawa, M. Ishida, T. Nakajima, Y. Honda, O. Kitao, H. Nakai, M. Klene, X. Li, J. E. Knox, H. P. Hratchian, J. B. Cross, V. Bakken, C. Adamo, J. Jaramillo, R. Gomperts, R. E. Stratmann, O. Yazyev, A. J. Austin, R. Cammi, C. Pomelli, J. Ochterski, P. Y. Ayala, K. Morokuma, G. A. Voth, P. Salvador, J. J. Dannenberg, V. G. Zakrzewski, S. Dapprich, A. D. Daniels, M. C. Strain, O. Farkas, D. K. Malick, A. D. Rabuck, K. Raghavachari, J. B. Foresman, J. V. Ortiz, Q. Cui, A. G. Baboul, S. Clifford, J. Cioslowski, B. B. Stefanov, G. Liu, A. Liashenko, P. Piskorz, I. Komaromi, R. L. Martin, D. J. Fox, T. Keith, M. A. Al-Laham, C. Y. Peng, A. Nanayakkara, M. Challacombe, P. M. W. Gill, B. G. Johnson, W. Chen, M. W. Wong, C. Gonzalez and J. A. Pople, *GAUSSIAN 03 (Revision C.02)*, Gaussian, Inc., Wallingford, CT, 2004.
27 M. Reiher, O. Salomon and B. A. Hess, *Theor. Chem. Acc.*, 2001, **107**, 48–55.
28 A. D. Becke, *J. Chem. Phys.*, 1993, **98**, 5648.
29 C. T. Lee, W. T. Yang and R. G. Parr, *Phys. Rev. B*, 1988, **37**, 785–789.
30 J. N. Harvey and M. Aschi, *Faraday Discuss.*, 2003, **124**, 129–143.

31 D. Andrae, U. Häußermann, M. Dolg, H. Stoll and H. Preuß, *Theor. Chim. Acta*, 1990, **77**, 123–141.
32 W. J. Hehre, R. Ditchfield and J. A. Pople, *J. Chem. Phys.*, 1972, **56**, 2257–2261.
33 M. F. Michelle, J. P. William, J. H. Warren, J. S. Binkley, S. G. Mark, J. D. Douglas and A. P. John, *J. Chem. Phys.*, 1982, **77**, 3654–3665.
34 S. Miertus, E. Scrocco and J. Tomasi, *Chem. Phys.*, 1981, **55**, 117–129.
35 C. Anda, A. Llobet, A. E. Martell, B. Donnadieu and T. Parella, *Inorg. Chem.*, 2003, **42**, 8545–8550.
36 C. Anda, A. Llobet, A. E. Martell, J. Reibenspies, E. Berni and X. Solans, *Inorg. Chem.*, 2004, **43**, 2793–2802.
37 C. Anda, A. Llobet, V. Salvado, J. Reibenspies, R. J. Motekaitis and A. E. Martell, *Inorg. Chem.*, 2000, **39**, 2986–2999.
38 J. P. Saucedo-Vázquez, V. M. Ugalde-Saldiívar, A. R. Toscano, P. M. H. Kroneck and M. E. Sosa-Torres, *Inorg. Chem.*, 2009, **48**, 1214–1222.
39 *CRC Handbook of Chemistry and Physics*, 84th edn, 2003.
40 L. Aronne, B. C. Dunn, J. R. Vyvyan, C. W. Souvignier, M. J. Mayer, T. A. Howard, C. A. Salhi, S. N. Goldie, L. A. Ochrymowycz and D. B. Rorabacher, *Inorg. Chem.*, 1995, **34**, 357–369.

